Chapter 1
Experimental Technique and Working Modes

Sascha Sadewasser and Thilo Glatzel

Abstract Kelvin probe force microscopy (KPFM) is a scanning probe microscopy technique providing the capability to image the surface potential of a sample with high spatial and energy resolution. It is based on non-contact atomic force microscopy (nc-AFM) and continuously minimizes the electrostatic interaction between the scanning tip and the surface. Compared to electrostatic force microscopy (EFM) which also measures the electrostatic properties KPFM compensates these force contributions. The two main working modes are the amplitude modulation and the frequency modulation technique, in which the electrostatic force or the electrostatic force gradient are minimized by the application of an appropriate dc-bias voltage, respectively. For metals and semiconductors, the contact potential difference is determined, which is related to the sample's work function, while for insulators information about local charges and dipoles is obtained. This chapter provides a brief introduction to nc-AFM, EFM, and various KPFM techniques.

1.1 Introduction

Surface science was revolutionized in 1982 by the invention of the scanning tunneling microscope (STM) by Binnig and Rohrer [1]. In 1986 the invention of the atomic force microscope (AFM) widened the range of samples from conductive to non-conductive ones [2]. Further development lead to the non-contact (or dynamic) mode of the AFM [3], where a cantilever supporting a sharp tip at its end is vibrated close to its resonance frequency and changes in the vibration due to tip-sample interaction are used to maintain a constant distance to the sample surface while

S. Sadewasser (✉)
International Iberian Nanotechnology Laboratory, Avenida Mestre Jos Veiga s/n,
4715-330 Braga, Portugal
e-mail: sascha.sadewasser@inl.int

T. Glatzel
Department of Physics, University of Basel, Klingelbergstr. 82, 4056 Basel, Switzerland
e-mail: thilo.glatzel@unibas.ch

© Springer International Publishing AG 2018

S. Sadewasser and T. Glatzel (eds.), *Kelvin Probe Force Microscopy*,
Springer Series in Surface Sciences 65, https://doi.org/10.1007/978-3-319-75687-5_1

scanning across the sample. Forces exerted by the tip on the sample are minimal in non-contact mode.

A wide field of applications has been opened by the combination of the AFM with other measurement methods, thus providing additional sample properties on a lateral scale in the nanometer range. The electrostatic interaction between tip and sample is measured by two AFM variations, the electrostatic force microscope (EFM) and the Kelvin probe force microscope (KPFM). In EFM, the electrostatic forces are measured qualitatively, while in KPFM a dc-bias voltage is applied between tip and sample to compensate the electrostatic forces. The KPFM was first developed by Nonnenmacher et al. [4] and it allows to image surface electronic properties, namely the contact potential difference (CPD). The name “Kelvin probe force microscope” originates from the macroscopic method developed by Lord Kelvin in 1898 using a vibrating parallel plate capacitor arrangement, where a voltage applied to one vibrating plate is controlled such that no current is induced by the vibration [5]. The reduction of this exact principle to the microscopic scale, however, results in a poor sensitivity, since the size of the capacitor plates is too small to generate a sufficient current. Therefore, in KPFM the electrostatic force is measured instead. The cantilever in an AFM is a very sensitive force sensor allowing to measure forces down to the pN range, thus the CPD can be measured with high spatial and energy sensitivity. A dc bias applied to the sample (or the tip) is controlled in such a way that the electrostatic forces between tip and sample are minimized.

This chapter will initially describe the working principle of non-contact atomic force microscopy (nc-AFM) and then explain the EFM and KPFM techniques. Two main working modes of KPFM will be described which are both widely applied in research laboratories. At the end of the chapter some notes on other working modes are given.

1.2 Non-contact Atomic Force Microscopy

An AFM consists of a sharp tip supported at the end of a cantilever serving as a force sensor [2]. The sample’s topography is imaged by scanning the tip across a sample surface while maintaining a constant force or force gradient by a feedback loop. Different modes for AFM operation can be used. In contact mode the tip is brought into contact with the sample, and repulsive tip-sample interaction is measured. In non-contact mode (also called dynamic mode) the tip is oscillated at or near its fundamental resonance frequency [3]. The oscillation is mechanically excited using a piezoelectric element on which the cantilever-chip is mounted. Interaction forces between tip and sample cause a shift in the resonance frequency. A third mode uses an oscillating cantilever, however, the regime of repulsive tip-sample interaction is reached in the lower turn-around point of the oscillation cycle, while in the rest of the oscillation cycle attractive forces dominate the interaction. In this tapping or intermittent contact mode and in the non-contact mode the forces exerted by the scanning tip on the sample are considerably reduced with respect to the contact mode.

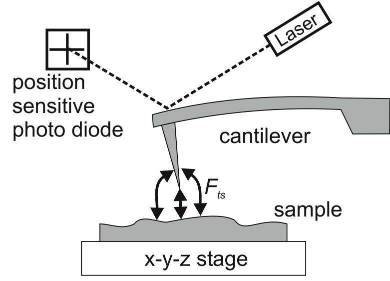

Fig. 1.1 Working principle of an AFM consisting of the beam deflection detection system with laser and position sensitive photodiode and the sample on a piezo-driven xyz-stage

In nc-AFM or dynamic AFM (DFM) the cantilever is oscillated at or near its resonance frequency and the change in the oscillation is monitored in dependence of the tip-sample interaction. Figure 1.1 shows the basic AFM experimental setup consisting of the cantilever and tip, the sample on a xyz-stage with piezo control, and the detection system with a laser and a position sensitive photodiode. Alternatively to the displayed beam-deflection detection an interferometric technique or a piezoelectric and piezoresistive detection can be used [6].

The oscillation of the cantilever can be described by its equation of motion, which in general is a three dimensional problem. By considering the tip as a point-mass spring the equation of motion for the tip can be represented as [7]:

$$m\ddot{z} + \frac{m\omega_0}{Q}\dot{z} + kz = F_{ts} + F_0 \cos(\omega_d t), \tag{1.1}$$

where k denotes the spring constant, Q the quality factor, F_{ts} the tip-surface interaction, F_0 and ω_d the amplitude and angular frequency of the driving force, respectively. The free resonance frequency f_0 (without tip-surface interaction, $F_{ts} = 0$) is a function of the spring constant k and the effective mass m^*, which also accounts for the specific geometry of the cantilever:

$$\omega_0 = 2\pi f_0 = \sqrt{\frac{k}{m^*}}. \tag{1.2}$$

When the tip is approached to the surface, forces act between tip and sample. This tip-surface interaction may consist of various contributions, short range repulsive and chemical binding forces, the van der Waals force F_{vdW}, and the long-range electrostatic and magnetic forces, F_{el} and F_{mag}, respectively. The short-range interaction is usually described by the empirical Lennard-Jones type interaction potential, which is illustrated in Fig. 1.2 [8]. The repulsive force in a distance r can be described by a power law interaction potential:

$$U_{rep} = \left(\frac{\sigma_0}{r}\right)^n, \tag{1.3}$$

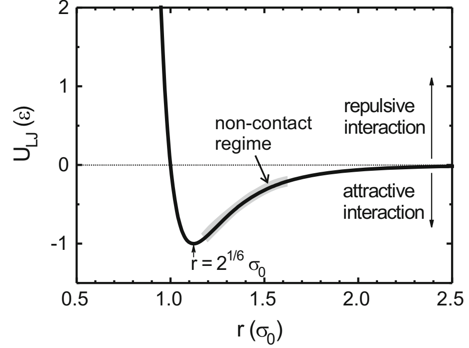

Fig. 1.2 Lennard-Jones type interaction potential describing the typical interaction of an AFM tip and the sample surface at small tip-sample distances

where the exponent is usually set to $n = 12$. Frequently, this repulsive part is also described by an exponential dependence:

$$U_{rep} = c \cdot \mathrm{e}^{-r/\sigma'}. \tag{1.4}$$

Here σ_0 and σ' are characteristic lengths, where σ' is on the order of 0.02 nm.

At larger distance, the interaction potential becomes attractive, goes through a minimum and then approaches zero towards large tip-sample distances. The total short-range interatomic interaction potential comprising the repulsive and attractive part can thus be described by a Lennard-Jones potential [8]:

$$U_{LJ} = -4\epsilon \left[\left(\frac{\sigma_0}{r} \right)^6 - \left(\frac{\sigma_0}{r} \right)^{12} \right], \tag{1.5}$$

as illustrated in Fig. 1.2.

The repulsive force at very small tip-sample distances results from the Pauli exclusion principle for the overlapping electron clouds of the tip and sample atoms. The chemical forces are due to the bonding state of a quantum mechanical overlap of the electron wave functions of tip and sample. These chemical interactions obey an exponential distance dependence and are only relevant at distances below ∼5 Å [9].

An additional contribution to the attractive part of the short-range interaction force is the van der Waals force. It is an always present interaction between atoms and molecules due to the interaction between induced electrostatic dipoles, i.e. as a result of electromagnetic field fluctuations. For the case of AFM, it can be approximated by considering a sphere of radius R in front of an infinite plane, representing the sample surface and is usually expressed as [7, 8]:

$$F_{vdW} = -\frac{HR}{6r^2}, \tag{1.6}$$

where H is the Hamaker constant, and r the closest distance between the sphere and the plane (the tip and the sample). For tip-sample distances smaller than an intermolecular distance a_0, F_{vdW} is replaced by the adhesion force F_{adh}. For the case of a stiff contact and a small tip radius the adhesion force can be described by $F_{adh} = -4\pi R\gamma$, where γ is the surface energy [7, 10, 11]. As indicated by the gray area of the interaction potential in Fig. 1.2, nc-AFM is typically operated in the attractive region of the interaction.

The relevant force for EFM and KPFM is the electrostatic force F_{el}. It can be expressed by considering the tip-sample system as a capacitor. Thus, with the energy of a capacitor, $U_{el} = 1/2CV^2$, the force can be written as:

$$F_{el} = -\nabla U_{el} = \frac{1}{2}\frac{\partial C}{\partial r}V^2 + CV\frac{\partial V}{\partial r}, \tag{1.7}$$

where C is the capacitance and V the total voltage. For simplicity, a metallic tip and sample can be considered. In the case of AFM, the most significant contribution is due to the forces perpendicular to the sample surface (denominated z-direction), therefore (1.7) simplifies to:

$$F_{el} = \frac{1}{2}\frac{\partial C}{\partial z}V^2, \tag{1.8}$$

which is always attractive because $\partial C/\partial z < 0$ [12], see also Chap. 8.3.3. A detailed discussion of the electrostatic force will follow in the next section. The magnetic forces are only relevant if tip and/or sample material are magnetic. Generally, for KPFM this is not the case and therefore these forces will not be considered here.

When approaching the tip to the sample, the interaction forces will cause a shift of the resonance curve of the cantilever. For small oscillation amplitudes the system can be regarded as a weakly perturbed harmonic oscillator. In this case the shift of the resonance curve can be approximated by introducing an effective spring constant k_{eff} [7]:

$$k_{eff} = k - \frac{\partial F_{ts}}{\partial z}. \tag{1.9}$$

The spring constant is lowered by the force gradient. For small force gradients this shifts the resonance curve, in the case of attractive forces to lower frequencies and vice versa. The frequency shift can be approximated by [7, 13]:

$$\Delta f_0 = -\frac{f_0}{2k}\frac{\partial F_{ts}}{\partial z}. \tag{1.10}$$

Equations (1.9) and (1.10) are approximations to the solution of the equation of motion (1.1) for small oscillation amplitudes and small force gradients. In many situations they provide a quick and easy way to interpret the experiments. However, in many practical cases of KPFM, large oscillation amplitudes are used, and thus throughout the oscillation cycle the tip-sample interaction continuously varies. The above approximations are no longer valid in this case and more elaborate methods

have to be used. In classical first-order perturbation theory the solution to the equation of motion gives the frequency shift Δf_0 as a function of the tip-sample distance d, the oscillation amplitude A_0, the spring constant k and the free resonance frequency f_0 as [7, 14]:

$$\Delta f_0 = -\frac{f_0}{kA_0^2}\frac{1}{T_0}\int_0^{T_0} F_{ts}\left(d + A_0 + A_0\cos(2\pi f_0 t)\right) A_0\cos(2\pi f_0 t)\,\mathrm{d}t. \tag{1.11}$$

Two different detection modes can be applied in AFM. Mainly in the intermittent contact mode the amplitude modulation technique is used [3] where the cantilever is excited at a constant frequency slightly off resonance. A change in the tip-sample distance leads to a change of the force gradient, which results in a shift of the resonance peak; thus, the oscillation amplitude at the fixed driving frequency changes. A feedback loop adjusts the tip-sample distance to maintain a constant amplitude. This detection method is usually applied in air, where the quality factor Q of the cantilever is on the order of 1–10^3. When operating an AFM in vacuum, the quality factor increases by several orders of magnitude (typically above 10^5) due to the reduced damping and the nc-AFM mode can be used. This results in a reduced bandwidth in the amplitude detection mode and a very slow response time of the system is the consequence [13]. Albrecht et al. [13] have introduced the frequency modulation technique (FM-mode) for tracking the resonance frequency in these cases. In this mode, the change of the resonance curve is detected by directly measuring the frequency shift of the resonance peak. The cantilever serves as the frequency determining element and is always excited at its resonance frequency using a feedback loop. Through an additional controller the oscillation amplitude is kept constant as well allowing to directly distinguish conservative and dissipative force contributions. The resonance frequency is measured using a frequency demodulator, or a phase locked loop (PLL), for example. For a change of the tip-sample distance during the scan the resonance frequency changes and the z-controller adjusts the tip-sample distance to maintain a constant frequency shift Δf_0 with respect to the free resonance of the cantilever. The experimental set-up of this FM-mode is illustrated in Fig. 1.5 in Sect. 1.4.3 below. For both modes, according to (1.10), the measured surface topography approximately corresponds to a surface of constant force gradient.

1.3 Electrostatic Force Microscopy

The electrostatic forces (1.7 and 1.8) contributing to the total force between cantilever and sample surface can be measured by electrostatic force microscopy (EFM). The most elegant way to separate the electrostatic from other force contributions is to modulate the force field by an ac-voltage $V_{ac} sin(\omega_{ac} t)$ at the frequency ω_{ac} inducing an electrostatically driven oscillation of the cantilever at the frequency ω_{ac}. This approach will also be valid for all major KPFM modes discussed later and will

therefore be introduced in more detail. Considering the tip-sample system as a capacitor, the electrostatic force in (1.8) can now be expressed as:

$$F_{el} = \frac{1}{2}\frac{\partial C}{\partial z}[V_{dc} - V_{CPD} + V_{ac}\sin(\omega_{ac}t)]^2, \tag{1.12}$$

where $\partial C/\partial z$ is the capacitance gradient of the tip-sample system and the CPD is the difference in work function Φ between sample and tip:

$$V_{CPD} = \Delta\Phi/e = (\Phi_{sample} - \Phi_{tip})/e, \tag{1.13}$$

where e is the elementary charge.[1] Equation (1.12) can be written as $F_{el} = F_{dc} + F_{\omega_{ac}} + F_{2\omega_{ac}}$, where the spectral components are:

$$F_{dc} = \frac{\partial C}{\partial z}\left[\frac{1}{2}(V_{dc} - V_{CPD})^2 + \frac{V_{ac}^2}{4}\right], \tag{1.14}$$

$$F_{\omega_{ac}} = \frac{\partial C}{\partial z}(V_{dc} - V_{CPD})V_{ac}\sin(\omega_{ac}t), \tag{1.15}$$

$$F_{2\omega_{ac}} = -\frac{\partial C}{\partial z}\frac{V_{ac}^2}{4}\cos(2\omega_{ac}t). \tag{1.16}$$

Here, F_{dc} induces an additional static force contribution influencing the topography signal, $F_{\omega_{ac}}$ modulated at the ac-frequency is used to measure the CPD in KPFM mode, and $F_{2\omega_{ac}}$ can be used for capacitance microscopy (see Sect. 1.4.4) [15]. The amplitude at the frequency ω_{ac} which can be detected by lock-in technique is therefore directly related to the magnitude of the electrostatic forces induced by the applied ac-voltage. By recording the magnitude of the lock-in signal variations of the electrostatic force can be measured. Typically EFM is performed in a two pass mode, measuring in the first pass the topography (typically including influences of the uncompensated electrostatic forces) and in the second pass lifting the cantilever typically several 10 nm up exciting the cantilever electrically or mechanically and measuring the electrostatic force while following the recorded topography trace with an applied dc-bias voltage offset [16]. A simultaneous measurement of the the topography and the electrostatic force signal is also possible by using different frequencies or even resonances for both channels. The acquired signal always contains influences from the capacitance gradient as well as the CPD and can therefore not easily be

[1] In principle, the definition of the CPD could also be selected as $V_{CPD} = (\Phi_{tip} - \Phi_{sample})/e$, which corresponds to $-V_{CPD}$ of (1.13). Typically the definition of (1.13) is selected such that the changes in V_{CPD} directly correspond to changes in the work function. Thus, images of V_{CPD} represent the same contrast as images of the sample's work function Φ_{sample}, just with a constant absolute offset, which is equal to the work function of the tip. In the experimental realization this would correspond to a situation, where the voltage is applied to the sample and the tip is grounded (see Sect. 1.4.3).

related with absolute work function values. Another clear disadvantage of the EFM beside the lack of a quantitative measurement of the CPD are the influences of the uncompensated electrostatic force on the topography [17, 18]. Nevertheless, the literature reports many EFM studies, likely motivated by the fact, that experimentally the EFM technique is simpler to handle and requires less equipment, namely it does not require an additional feedback loop, as does KPFM.

1.4 Kelvin Probe Force Microscopy

KPFM combines nc-AFM and EFM with the Kelvin probe technique. The macroscopic Kelvin technique was developed in 1898 by Kelvin [5] for the measurement of surface potentials: the sample constitutes one plate of a parallel plate capacitor, with a known metal forming the other plate, which is vibrated at frequency ω. Due to the changing distance between the plates, the capacitance changes, resulting in an alternating current in the circuit connecting the plates. This current is reduced to zero by applying a dc-voltage to one of the plates. This voltage corresponds to the contact potential difference of the two materials.

The KPFM employs the same principle, applying a dc-voltage to compensate the CPD between the AFM tip and the sample [19]. However, instead of the current as the controlling parameter, the electrostatic force is used as described above for the EFM. As the cantilever of an AFM is a very sensitive force probe, this technique results in a high sensitivity of the CPD measurement, even for the very reduced size of the capacitor formed by the tip and the sample. Compared to EFM, in KPFM an additional dc-voltage (V_{dc}) between tip and sample is applied to minimize the electrostatic forces resulting in a zero amplitude at the frequency ω, see (1.15). For that purpose an additional feedback loop is required.

While the KPFM measurement results in the determination of the CPD, which is the work function of the sample relative to that of the tip, (1.13) can be used to deduce the sample's work function on an absolute scale. Using a calibrated tip with a known work function, the work function of the sample can be calculated from the CPD measurement according to (1.13). However, for absolute work function measurements, operation under ultra-high vacuum (UHV) conditions is mandatory [20], as it is well known that the work function is highly sensitive to the surface cleanness [4].

As in the case of the topography measurement, also for the CPD measurement two different modes can be distinguished. The amplitude modulation technique (AM-mode) controls the applied dc-bias by reducing the amplitude of the induced oscillation at the ac-frequency to zero, and the frequency modulation technique (FM-mode) minimizes the variation in the frequency shift Δf_0 at the ac-frequency.

1.4.1 AM-KPFM

In the AM-mode, the amplitude of the cantilever oscillation at the ac-frequency ω_{ac} is measured; it is induced by the electrostatic force and is proportional to it. The amplitude is detected using the beam deflection signal and a lock-in amplifier tuned to the frequency of the ac-bias (see also Sect. 1.4.3). As can be seen from (1.15), this signal is minimized by controlling V_{dc} to match the contact potential difference V_{CPD}. Recording V_{dc} while scanning the topography, an image of the CPD is obtained. Some KPFM systems use this technique with ac-frequencies of several kHz to several tens of kHz. To get sufficient sensitivity, ac-voltages of 1–3 V are typically used [21, 22].

An improvement to this technique is obtained by tuning the ac-frequency to an eigenmode of the cantilever. In this way a resonance-enhanced detection is achieved, providing the possibility to lower the ac-voltage maintaining a high sensitivity to the electrostatic force. An elegant way to use resonance-enhanced KPFM is to tune the ac-frequency to the second eigenmode of the cantilever [23, 24]. While the fundamental resonance is mechanically excited and used for topography detection, the ac-voltage simultaneously excites electrostatically a cantilever oscillation, for example of the second eigenmode, which is used for the CPD detection. Then the oscillation at ω_{ac} is amplified by the quality factor Q of the respective eigenmode. This enhances the sensitivity and permits to use lower ac-voltages, down to the order of 100 mV. Working with the resonance-enhanced detection, also the response time of the system is determined by the quality factor. This can be quantitatively expressed in a similar way as for the fundamental resonance used for the topography detection [13]. The system reacts to a change (for example a change in the CPD upon scanning the tip) with a response time τ until a new stable state is reached, where [13, 25]:

$$\tau = \frac{Q}{\pi f_2}. \quad (1.17)$$

Using typical values of $Q = 5000 - 15000$ and $f_2 = 450 - 1200\,kHz$ the response time results to a view ms. This means that scanning is easily possible with scan speeds on the order of SI1s/line.

The limiting factor in this mode is the bandwidth of the photodiode used for the detection of the cantilever oscillation. This bandwidth depends on the specific type and manufacturer of the AFM system. In many commercial systems a photodiode with a bandwidth of ~500 kHz is used; therefore, the stiffest cantilevers used for detection on the second oscillation mode have the fundamental resonance frequency in the range of 70–80 kHz, and the second resonance around 400–470 kHz ($f_2 \sim 6.3 f_0$, due to the geometry of the cantilever [26]). Typical resonance curves for the fundamental and second oscillation mode are shown in Fig. 1.3. The amplitude of the second resonance mode is smaller by about a factor of 10 when the same excitation amplitude is used for the mechanical excitation of the dither-piezo.

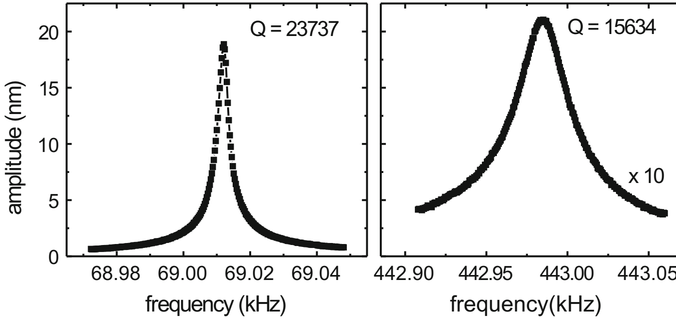

Fig. 1.3 Resonance peaks of the fundamental and second eigenmode of a typical cantilever for force modulation AFM (Nanosensors PPP-EFM). The Q-factors for the two resonances are also given

Thus, the resonance-enhanced AM-mode KPFM has two advantages: (i) a simultaneous measurement of topography and CPD is possible due to the use of two independent resonance modes and (ii) the resonance enhancement provides a higher sensitivity to the electrostatic force and therefore allows to use smaller ac-voltages. This in turn has two additional advantages. First, the ac-amplitude affects the topography image by inducing a constant electrostatic background, as can be seen by the $V_{ac}^2/4$-term in (1.14). Second, large ac-voltages possibly induce band bending at the surface of semiconductors [27], which would cause an incorrect determination of the work function.

1.4.2 FM-KPFM

In the frequency modulation mode, the applied ac-bias voltage induces a modulation of the electrostatic force, which results in an oscillation of the frequency shift Δf_0 at the frequency f_{ac} of the ac-bias. This oscillation is detected by a lock-in amplifier tuned to the frequency of the ac-bias. The measured signal is approximately proportional to the force gradient, as can be concluded from (1.10) and (1.15):

$$\Delta f_0(\omega_{ac}) \propto \frac{\partial F_{\omega_{ac}}}{\partial z} = \frac{\partial^2 C}{\partial z^2}(V_{dc} - V_{CPD})V_{ac}\sin(\omega_{ac}t). \qquad (1.18)$$

As was shown in [28], the frequency ω_{ac} has to be chosen in an appropriate range. The lower limit is dictated by an increasing crosstalk to the topography signal: if the frequency is too low, the tip-sample distance control follows the additional electrostatic force and the tip-sample distance starts to oscillate at the frequency ω_{ac}. The higher the frequency the lower the coupling to the topography. On the other hand, the bandwidth of the frequency demodulator or the PLL determines the upper limit

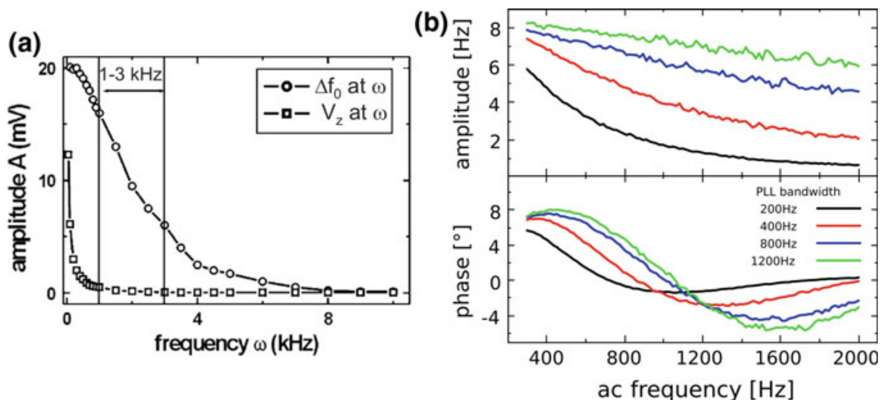

Fig. 1.4 **a** Dependence of the amplitude of the frequency shift Δf_0 and the height control signal of the topography, V_z, at the frequency ω of the ac voltage. The measurements were obtained on a HOPG sample with a bias slightly above the CPD using a room temperature UHV-AFM system by Omicron Nanotechnology, reprinted from Publication Appl. Surf. Sci. 210, 84, (2003), with permission from Elsevier [28]. **b** Amplitude and phase dependence of the frequency shift Δf_0 at the ac frequency ω_{ac} from the PLL bandwidth of the phase controller experimentally obtained with a metal-coated cantilever on a Cu(111) sample with a Nanonis Control System (RC 4.5)

of the frequency range. Figure 1.4a shows the amplitudes at ω_{ac} of the oscillation of Δf_0 and of the oscillation of the piezo voltage V_z, which controls the tip-sample distance as well as the dependence of the signal on the demodulator bandwidth. With increasing frequency ω_{ac} the crosstalk to the topography signal decreases but also the signal intensity of the electrostatic force decreases due to the restricted bandwidth of the frequency demodulator. Also in this mode, higher V_{ac} results in higher sensitivity at the cost of an influence on the topography and a possibly induced band bending on semiconductor samples (see above). Typical values for $f_{ac} = \omega_{ac}/2\pi$ and V_{ac} are in the range of 1–3 kHz and 1–3 V, respectively. Increasing the bandwidth of the PLL by tuning the phase controller time constant to higher frequencies allows to use higher ac frequencies f_{ac} as presented for four different values in Fig. 1.4b. The data have been measured with a metal coated cantilever on a Cu(111) surface with a UHV-AFM at room temperature by a Nanonis Control System (RC 4.5). A typical bandwidth for high resolution measurements is 200 Hz which allows still fast enough measurements by rejecting high frequency noise.

1.4.3 Technical Realization

Figure 1.5 shows a typical setup of the electronic system of a KPFM. The cantilever oscillation is detected by a beam deflection method using a laser, reflected from the backside of the cantilever onto a position sensitive photodiode. The signal is fed

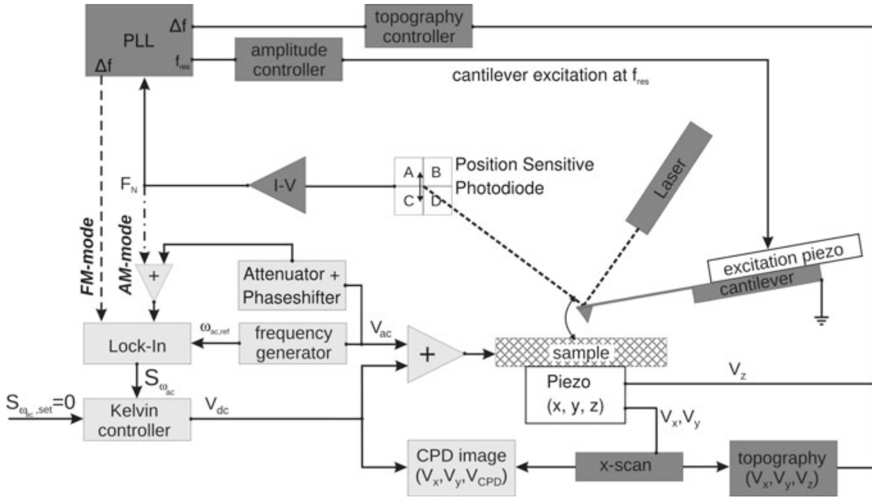

Fig. 1.5 Block diagram of the electronic realization of a KPFM. The dashed line indicates the FM-mode and the dashed-dotted line the AM-mode setup. Dark grey boxes are the regular non-contact AFM topography part and the light gray boxes are the KPFM part of the setup. In the AM-KPFM part an additional attenuator combined with a phase shifter can be used to compensate for capacitive crosstalk. See text for details

into a frequency detector, as for example a phase locked loop (PLL) or a frequency demodulator, which mechanically excites the cantilever oscillation on the fundamental resonance frequency f_{res}. For the detection of the electrostatic forces a frequency generator feeds the desired ac-voltage into an adder element, and at the same time provides the reference frequency for the lock-in amplifier. Depending on the used lock-in amplifier, also the reference output voltage can be used directly as the ac bias for the sample. In FM-mode KPFM, the Δf_0 signal from the PLL is directly fed into the lock-in amplifier (see dashed arrow in Fig. 1.5), which then detects the magnitude of the frequency shift at the ac frequency, induced by the electrostatic forces. The lock-in output, the x-component or the in-phase signal after appropriate phase adjustment, serves as input to the Kelvin controller, which adjusts a dc voltage such that the input signal ($S_{\omega_{ac}}$) goes towards zero. This dc voltage V_{dc} is the second input to the adder, which provides then the complete voltage to the sample, consisting of the sum of ac- and dc-bias. On the other hand, as was shown above, the dc-bias matches the CPD and thus the dc-bias is recorded with the scan to provide the spatially resolved CPD image.

Figure 1.5 shows also the setup for the AM-mode KPFM. In this case, the output signal from the position sensitive photodiode is connected to the input of the lock-in amplifier, as shown by the dashed-dotted line in Fig. 1.5. The rest of the setup is identical to the FM-mode setup. Thus, in the AM-mode, the amplitude of the induced oscillation of the cantilever is measured directly, as described above in Sect. 1.4.1. For a better separation of the fundamental resonance frequency from the

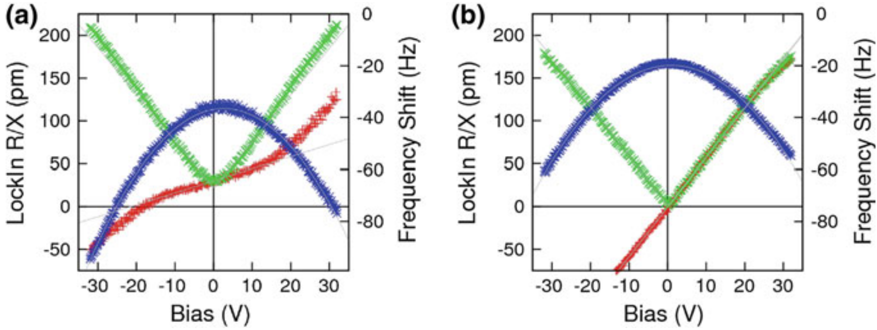

Fig. 1.6 Frequency shift (blue) and lock-in signals (amplitude (green) and x-component or in-phase signal (red)) used for KPFM. The in-phase signal is used as in input for the Kelvin controller. **a** A capacitive crosstalk might induce an offset in the amplitude and in-phase signal, leading to a false CPD value. A phase change or inappropriate adjusted phase might even enhance this effect. **b** This error can and should be compensated by an appropriate circuit if necessary, see Fig. 1.5, since already small offsets can induce severe changes and artefacts in the measured CPD

ac-frequency signal from the photodiode a high and/or low-pass filter might optionally by used. AM-KPFM measurements can be influenced by capacitive crosstalk between the ac-bias voltage and the deflection output signal of the photodiode or the z-piezo signal [27, 29, 30]. As depicted in Fig. 1.6a this kind of crosstalk results in an offset of the detected KPFM signal. The main KPFM signal is the measured amplitude *R* (green) which is shifted up to positive values inducing also a shift of the x-component used as the input for the Kelvin controller. As can be seen in the red curve in Fig. 1.6a this will result in a false CPD value which can even be enhanced by an inappropriate phase adjustment. The best way to reduce this capacitive coupling is an appropriate shielding of the signal lines inside the UHV chamber as well as different feedthroughs for signal and bias lines [27, 31]. As shown by Diesinger et al. [30] an additional active compensation of the crosstalk by an externally applied ac-bias reduces the crosstalk down to the noise level [29]. This ac-bias crosstalk compensation needs to have exactly the same frequency ω_{ac} as the ac-bias excitation and its phase and amplitude are fitted to the capacitive crosstalk measured between the photodiode and the Kelvin signal. However, for well-shielded AFM systems such crosstalk influences are negligible especially for measurements on metallic or semiconducting samples since the strength of the elctrostatic forces (slope of the lock-in amplitude in Fig. 1.6) is strongly enhanced compared to insulating surfaces like KBr used for the measurements in Fig. 1.6, which might induce CPD-offsets of several V.

1.4.4 Other Modes and Additional Experimental Options

The capability of KPFM to acquire images of the CPD relies on (1.15), as discussed above. A closer examination of (1.15) shows that the electrostatic force component at the ac frequency ω_{ac} not only exhibits the dependence on the voltage difference $(V_{dc} - V_{CPD})$, but also a possible contribution of the capacitance gradient $\partial C/\partial z$ has to be considered. Local variations of this contribution possibly affect measurements. This effect should be severe for EFM imaging, where the CPD is not compensated and therefore variations in the EFM signal obtained from the lock-in amplifier might erroneously be attributed to CPD variations. However, the effect on KPFM images should be much smaller or even negligible, as the Kelvin controller reduces the $(V_{dc} - V_{CPD})$ part of (1.15) to zero. Therefore, the $\partial C/\partial z$ contribution should not affect AM or FM-KPFM imaging. Moreover, considering (1.16), it is seen that by monitoring the induced oscillation of the cantilever at the frequency $2\omega_{ac}$ it becomes possible to aquire an image of $\partial C/\partial z$ [32, 33]. In the case of applying the FM-mode imaging, the corresponding second derivative would be imaged: $\partial C^2/\partial^2 z$. As (1.16) is independent of the applied dc-bias V_{dc} and V_{CPD}, the only dependence of this force component stems from variations in the capacitance gradient. In the experimental set-up, such a measurement can be realized by using an additional lock-in amplifier with the reference tuned to $2\omega_{ac}$, which then as an output signal provides the capacitance gradient [15].

Hochwitz et al. [15] have used this capacitance imaging to study complementary metal-oxide-semiconductor (CMOS) gates. Comparing individual devices in a CMOS chip, the monitored CPD did not show a clear distinction between properly functioning gates and gates that failed in operation. However, the capacitance gradient provided a clear signal difference between functional and non-functional CMOS gates. The authors concluded therefore, that the mechanism for the failure is beneath the surface. While the KPFM imaging is highly surface sensitive, the capacitance gradient provides also information from a region below the surface.

The subsurface sensitivity of the capacitance imaging is explained by the fact that for semiconductors the application of the ac-bias V_{ac} affects the charge distribution at the surface and subsurface region below the tip. Depending on the doping type of the sample and whether the ac-bias is in the positive or negative half of the oscillation cycle, the surface will undergo accumulation or depletion, respectively. The magnitude of the resulting change in the capacitance gradient depends on the charge carrier concentration [16, 34], similar to the way scanning capacitance microscopy works [35].

Recently several publications appeared using the so called Kelvin probe force spectroscopy (KPFS) method based on the fact that dynamic compensation during measurement is hindered by strong electrical coupling of the used tuning fork sensors [36–47]. This method can also be beneficial for cantilever based systems as for example presented on a Si(111) surface by Sadewasser et al. [48]. Figure 1.7 shows the basic principle of these measurements. First an area of interest is located and a grid of specific measurement points is defined. In between every single measurement

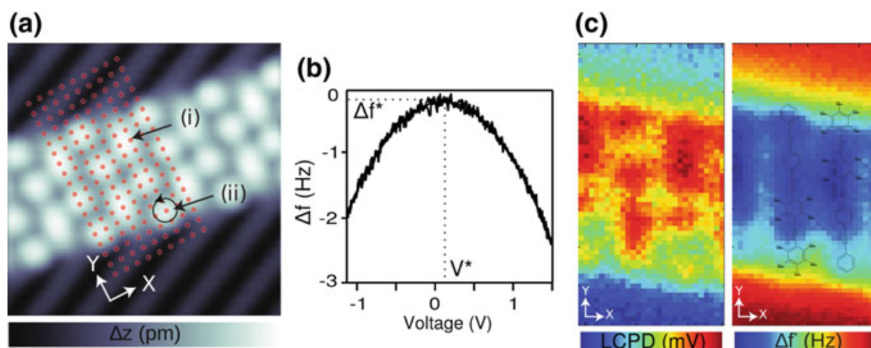

Fig. 1.7 Kelvin probe force spectroscopy. **a** The area of interest is selected and a grid of measurement points (i) is defined. To avoid thermal drift the relative tip-sample position can be adjusted by atom tracking (e.g. at position (ii)). **b** Example of a single bias-voltage dependent curve of the frequency shift. **c** Two dimensional maps of the extracted local contact potential difference (V^*) and the frequency shift at the CPD (Δf^*) calculated with a parabolic fit. Adapted with permission from ACS Nano 7, 9098 (2013) [36]. Copyright (2013) American Chemical Society

(i) an atom-tracking step (ii) [49] might be used to avoid thermal drift artefacts even at temperatures as low as 5K. In every point a dc-bias spectroscopy will be performed at constant height and the resulting frequency shift curve as shown in Fig. 1.7b will be fitted by a parabolic function to extract the coordinates V^* and Δf^* of the maximum. V^* corresponds to the LCPD while Δf^* is the frequency shift corresponding to the electronically uninfluenced interaction force. The results for such a measurement on a molecular assembly of donor-acceptor molecules arranged on a Au(111) surface are presented in Fig. 1.7c [36].

Another interesting new KPFM mode is the so called dissipation KPFM (D-KPFM) presented recently by Miyahara et al. [50, 51] and also discussed in detail in Chap. 2. This technique enables force and force-gradient sensitive KPFM by using the dissipation signal of standard nc-AFM for the dc-bias voltage feedback. It avoids low ac-voltage frequency oscillation and the need of an additional lock-in detection circuit enabling faster scanning and a straight-forward implementation. However, specific attention has to be paid to the correct adjustment of the excitation phase and occurring dissipation due to inelastic tip-sample interactions. The resulting CPD values are comparable to the ones obtained by the AM- or FM-KPFM techniques.

One way to avoid completely the compensation or even application of a dc-bias voltage is the so called open-loop KPFM approach. This technique was presented by N. Kobayashi et al. in 2010 focusing on the need to measure surface potentials in liquid environments [52, 53]. It is based on the measurement of the two electrostatically excited components ω_{ac} and $2\omega_{ac}$ and the calculation of the CPD by eliminating the influence of the capacitance gradient. Therefore, this approach is not only limited to the application to liquids but can also be applied to sensitive samples like insulators or low-doped semiconductors to avoid dc-bias induced effects. Many details and different approaches for the accurate detection can be found in several chapters

of this book: band excitation and G-mode KPFM in Chap. 3 by S. Jesse et al., an introduction to liquid KPFM in Chap. 4 by K. Kobayashi et al., and the application of liquid KPFM in Chap. 13 by L. Collins et al.

1.5 Additional Remarks

Due to the extremely short-range nature of the tunneling current, the scanning tunneling microscope provides a high sensitivity to the sample topography; the tunneling current passes almost exclusively through the outer-most tip atom. In contrast to this, in KPFM the electrostatic forces are relevant for the imaging process. Since those have a long-range character, it is not anymore the outer-most tip atom, but the whole tip, which determines the interaction between tip and sample, possibly also the cantilever itself. Therefore, the tip shape plays a role in KPFM imaging and several authors have studied the influences. Colchero et al. [54] have analytically investigated the influence of the tip and the cantilever in electrostatic force microscopy. Based on their analysis, the cantilever plays an important role in EFM and AM-KPFM imaging, despite the fact that the distance between cantilever and sample is $\sim 10^4$ times larger than the distance between the tip apex and the sample. However, due to the much larger surface area of the cantilever with respect to the tip apex, its role remains important. Their suggestion to avoid a reduction in spatial resolution due to interaction with the cantilever is to use FM-KPFM. Due to the shorter interaction range of the force gradient, the influence of the cantilever is considerably reduced, providing a better spatial resolution. This was later confirmed quantitatively by Zerweck et al. [55], who performed finite element simulations to describe the electrostatic interaction between the tip and a sample and extract the spatial resolution from scan lines of model structures. Basically, the resolution in FM-mode imaging is limited by the tip radius [56, 57]. However, both studies did not consider the resonance-enhanced AM-mode KPFM, which in many experimental studies has also provided very high resolution on the order of the tip radius [31, 58], even down to the submolecular and atomic scale [59–62].

The influence of the cantilever on EFM and KPFM imaging was also studied by investigating the dependence of the relative contribution of the capacitance derivative for the tip and the cantilever. Hochwitz et al. [63] numerically simulated the influence of the tip-to-cantilever area and the relative tip-to-cantilever distance to the sample on the ratio $\left(\partial C_{tip}/\partial z\right) / \left(\partial C_{cantilever}/\partial z\right)$. The relative area of the cantilever to the tip was varied between 10^1 and 10^9 and the ratio between the tip-sample distance and the cantilever-sample distance was varied between 10^{-1} and 10^{-4}. As is shown in Fig. 1.8a, the ratio of tip to cantilever capacitance gradient varies in form of a relative sharp step function. The authors find an optimal working region for KPFM or EFM with the cantilever to tip area in the range between 10^3 and 10^6 and the tip-sample distance to cantilever-sample distance to be less than 10^{-3}. This last criterion means that for a typical tip height of $\sim 10\ \mu$m a tip-sample distance of 10 nm or less

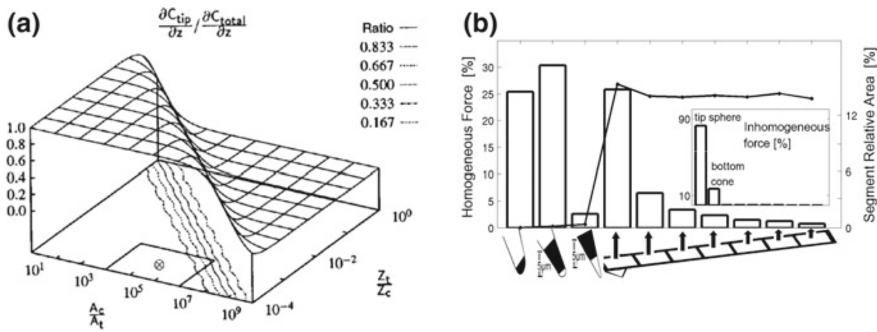

Fig. 1.8 **a** Surface plot showing the relative contribution of the tip/sample capacitance compared to the total probe/sample capacitance as functions of the area and sample spacing over a topographically flat surface. A_c/A_t is the ratio of the cantilever area to the tip area and Z_t/Z_c is the ratio of the tip-sample distance to the cantilever-sample distance. Reprinted with permission from J. Vac. Sci. Technol. B 14, 457, (1996) [63]. Copyright 1996, American Vacuum Society. **b** Role of the cantilever in quantitative Kelvin probe force microscopy (KPFM) using the boundary element method to calculate the point spread function of the entire probe. The figure shows that the cantilever has a very strong effect on the absolute value of the measured contact potential difference but the spatial resolution is mainly restricted by the front most part of the tip. Reprinted with permission from Beilstein Journal of Nanotechnology 2, 252,(2011) [64]

should be maintained. On the other hand, the first criterion leads to the conclusion, that the intuitive guess that a finer tip results in a finer resolution only applies to a certain limit. If the tip gets too sharp, a decrease in resolution results, since the ratio of cantilever area to tip area increases. Thus, long, slender, and slightly blunt tips should provide better resolution [63].

An experimental study confirming the simulations of Hochwitz et al. [63] was presented by Glatzel et al. [28]. Different cantilever types were comparatively used for the imaging of gold islands on a HOPG substrate. For the nominally same tip radius, short tips provide less potential contrast between Au and HOPG as compared to measurements with tips with a 3–5 times larger tip height. For the latter tips, the cantilever is further away from the sample and therefore the averaging due to the long-range electrostatic force is reduced. Experimentally, the CPD contrast between gold and graphite was about twice as large for the longer tips. Furthermore, as shown in Fig. 1.8b, it was shown by Elias et al. [64] that different parts of the cantilever beam and the tip cone have weighted contributions to the spatial and energy resolution. While the spatial resolution is mainly influenced by the tip apex size the energy resolution is also influenced by the cantilever beam.

Sadewasser and Lux-Steiner [17] showed the impact of the electrostatic forces on the topography imaging with regular nc-AFM imaging at fixed sample bias. For a fixed sample bias the electrostatic force acting on the tip is different depending on the local CPD under the present tip position, as can be seen from (1.12). Thus, these uncompensated electrostatic forces contribute to the topography contrast, in addition to the van-der-Waals forces. For a sample consisting of only two materials

with different CPD, correct topography imaging is possible, when the sample bias is selected to correspond to the average CPD of the two materials. However, for more than two materials, it is not possible to apply a fixed bias and maintain a correct imaging of the topography in nc-AFM [17]. In such a case, KPFM has to be used to provide a local compensation of the electrostatic forces and allow imaging of the topography based on purely van der Waals forces. These conclusions apply to KPFM imaging in the AM- as well as in the FM-mode. Thus, KPFM not only allows imaging the CPD structure of a sample, but also provides for a topography imaging free from the influence of electrostatic forces. The relevance of electrostatic forces for topography imaging in nc-AFM was also addressed by Dianoux et al. [65].

References

1. G. Binnig, H. Rohrer, C. Gerber, E. Weibel, Phys. Rev. Lett. **49**(1), 57 (1982)
2. G. Binnig, C. Quate, C. Gerber, Phys. Rev. Lett. **56**(9), 930 (1986)
3. Y. Martin, C. Williams, H. Wickramasinghe, J. Appl. Phys. **61**(10), 4723 (1987)
4. M. Nonnenmacher, M.P. O'Boyle, H.K. Wickramasinghe, Appl. Phys. Lett. **58**(25), 2921 (1991)
5. L. Kelvin, Phil. Mag. **46**, 82 (1898)
6. S. Morita, F.J. Giessibl, E. Meyer, R. Wiesendanger (eds.), *Noncontact Atomic Force Microscopy* (Springer International Publishing, 2015). https://doi.org/10.1007/978-3-319-15588-3
7. R. García, R. Pérez, Surf. Sci. Rep. **47**, 197 (2002)
8. J.N. Israelachvili, *Intermolecular and Surface Forces* (Elsevier LTD, Oxford, 2011)
9. R. Pérez, M. Payne, I. Stich, K. Terukura, Phys. Rev. Lett. **78**, 678 (1997)
10. L. Zitzler, S. Herminghaus, F. Mugele, Phys. Rev. B **66**, 155436 (2002). https://doi.org/10.1103/PhysRevB.66.155436
11. B. Derjaguin, V. Muller, Y. Toporov, J. Colloid Interface Sci. **53**(2), 314 (1975). https://doi.org/10.1016/0021-9797(75)90018-1
12. A. Sadeghi, A. Baratoff, S.A. Ghasemi, S. Goedecker, T. Glatzel, S. Kawai, E. Meyer, Phys. Rev. B **86**, 075407 (2012). https://doi.org/10.1103/PhysRevB.86.075407
13. T. Albrecht, P. Grütter, D. Horne, D. Rugar, J. Appl. Phys. **69**(2), 668 (1991)
14. F. Giessibl, Phys. Rev. B **56**(24), 16010 (1997)
15. T. Hochwitz, A. Henning, C. Levey, C. Daghlian, J. Slinkman, J. Never, P. Kaszuba, R. Gluck, R. Wells, J. Pekarik, R. Finch, J. Vac. Sci. Technol. B **14**(1), 440 (1996)
16. P.A. Rosenthal, E.T. Yu, R.L. Pierson, P.J. Zampardi, J. Appl. Phys. **87**(4), 1937 (1999)
17. S. Sadewasser, M. Lux-Steiner, Phys. Rev. Lett. **91**, 266101 (2003)
18. M. Yan, G.H. Bernstein, Ultramicroscopy **106**(7), 582 (2006). https://doi.org/10.1016/j.ultramic.2006.02.002
19. J. Weaver, D. Abraham, J. Vac. Sci. Technol. B **9**(3), 1559 (1991)
20. A. Kikukawa, S. Hosaka, R. Imura. Appl. Phys. Lett. **66**(25), 3510 (1995)
21. R. Shikler, T. Meoded, N. Fried, B. Mishori, Y. Rosenwaks, J. Appl. Phys. **86**(1), 107 (1999)
22. R. Shikler, T. Meoded, N. Fried, Y. Rosenwaks, Appl. Phys. Lett. **74**(20), 2972 (1999)
23. C. Sommerhalter, *Kelvinsondenkraftmikroskopie im Ultrahochvakuum zur Charakterisierung von Halbleiter-Heterodioden auf der Basis von Chalkopyriten* (Dissertation, Freie Universitt Berlin, 1999)
24. A. Kikukawa, S. Hosaka, R. Imura, Rev. Sci. Instrum. **67**(4), 1463 (1996)
25. S. Kawai, H. Kawakatsu, Appl. Phys. Lett. **89**, 013108 (2006). https://doi.org/10.1063/1.2219415

26. H.J. Butt, M. Jaschke, Nanotechnology **6**, 1 (1995)
27. C. Sommerhalter, T. Glatzel, T. Matthes, A. Jäger-Waldau, M. Lux-Steiner, Appl. Surf. Sci. **157**, 263 (2000)
28. T. Glatzel, S. Sadewasser, M. Lux-Steiner, Appl. Sur. Sci. **210**, 84 (2003)
29. T. Glatzel, Kelvin probe force microscopy for solar cell applications. Scanning Probe Microscopy for Energy Research, vol. 7 (World Scientific Pub Co, 2013)
30. H. Diesinger, D. Deresmes, J.P. Nys, T. Melin, Ultramicroscopy **108**, 773 (2008). https://doi.org/10.1016/j.ultramic.2008.01.003
31. C. Sommerhalter, T.W. Matthes, T. Glatzel, A. Jäger-Waldau, M.C. Lux-Steiner, Appl. Phys. Lett. **75**(2), 286 (1999)
32. Y. Martin, D. Abraham, H. Wickramasinghe, Appl. Phys. Lett. **52**(13), 1103 (1988)
33. D. Abraham, C. Williams, J. Slinkman, H. Wickramasinghe, J. Vac. Sci. Technol. B **9**(2), 703 (1991)
34. F. Müller, A.D. Müller, M. Hietschold, S. Kämmer, Meas. Sci. Technol. **9**, 734 (1998)
35. C. Williams, Annu. Rev. Mater. Sci. **29**, 471 (1999). https://doi.org/10.1146/annurev.matsci.29.1.471
36. S. Kawai, A. Sadeghi, X. Feng, P. Lifen, R. Pawlak, T. Glatzel, A. Willand, A. Orita, J. Otera, S. Goedecker, E. Meyer, ACS Nano **7**(10), 9098 (2013). https://doi.org/10.1021/nn403672m
37. L. Gross, F. Mohn, P. Liljeroth, J. Repp, F.J. Giessibl, G. Meyer, Science **324**(5933), 1428 (2009). https://doi.org/10.1126/science.1172273
38. T. Knig, G.H. Simon, H.P. Rust, G. Pacchioni, M. Heyde, H.J. Freund, J. Am. Chem. Soc. **131**, 17544 (2009). https://doi.org/10.1021/ja908049n
39. F. Mohn, L. Gross, N. Moll, G. Meyer, Nat. Nano **7**(4), 227 (2012)
40. L. Gross, B. Schuler, F. Mohn, N. Moll, N. Pavliček, W. Steurer, I. Scivetti, K. Kotsis, M. Persson, G. Meyer, Phys. Rev. B **90**, 155455 (2014). https://doi.org/10.1103/PhysRevB.90.155455
41. B. Schuler, S.X. Liu, Y. Geng, S. Decurtins, G. Meyer, L. Gross, Nano Lett. **14**(6), 3342 (2014). https://doi.org/10.1021/nl500805x
42. W. Steurer, J. Repp, L. Gross, I. Scivetti, M. Persson, G. Meyer, Phys. Rev. Lett. **114**, 036801 (2015). https://doi.org/10.1103/PhysRevLett.114.036801
43. R. Pawlak, T. Glatzel, V. Pichot, L. Schmidlin, S. Kawai, S. Fremy, D. Spitzer, E. Meyer, Nano Lett. **13**(12), 58035807 (2013). https://doi.org/10.1021/nl402243s
44. R. Pawlak, A. Sadeghi, R. Jöhr, A. Hinaut, T. Meier, S. Kawai, Ł. Zajac, P. Olszowski, S. Godlewski, B. Such, T. Glatzel, S. Goedecker, M. Szymoński, E. Meyer, J. Phys. Chem. C **121**(6), 3607 (2017). https://doi.org/10.1021/acs.jpcc.6b11873
45. P. Hapala, M. Švec, O. Stetsovych, N.J. van der Heijden, M. Ondráček, J. van der Lit, P. Mutombo, I. Swart, P. Jelnek, Nat. Commun. **7**, 11560 (2016). https://doi.org/10.1038/ncomms11560
46. F. Albrecht, J. Repp, M. Fleischmann, M. Scheer, M. Ondráĉek, P. Jelínek, Phys. Rev. Lett. **115**(7) (2015). https://doi.org/10.1103/physrevlett.115.076101
47. F. Albrecht, M. Fleischmann, M. Scheer, L. Gross, J. Repp, Phys. Rev. B **92**, 235443 (2015). https://doi.org/10.1103/PhysRevB.92.235443
48. S. Sadewasser, C. Leendertz, F. Streicher, M.C. Lux-Steiner, Nanotechnology **20**, 505503, (2009). https://doi.org/10.1088/0957-4484/20/50/505503
49. D.W. Pohl, R. Möller, Rev. Sci. Instrum. **59**(6), 840 (1988). https://doi.org/10.1063/1.1139790
50. Y. Miyahara, J. Topple, Z. Schumacher, P. Grutter, Phys. Rev. Appl. **4**(5) (2015). https://doi.org/10.1103/physrevapplied.4.054011
51. Y. Miyahara, P. Grutter, Appl. Phys. Lett. **110**(16), 163103 (2017). https://doi.org/10.1063/1.4981937
52. N. Kobayashi, H. Asakawa, T. Fukuma, Rev. Sci. Instrum. **81**(12), 123705 (2010). https://doi.org/10.1063/1.3514148
53. N. Kobayashi, H. Asakawa, T. Fukuma, J. Appl. Phys. **110**(4), 044315 (2011). https://doi.org/10.1063/1.3625230
54. J. Colchero, A. Gil, A. Baró, Phys. Rev. B **64**, 245403 (2001)

55. U. Zerweck, C. Loppacher, T. Otto, S. Grafström, L. Eng, Phys. Rev. B **71**, 125424 (2005). https://doi.org/10.1103/PhysRevB.71.125424
56. F. Krok, K. Sajewicz, J. Konior, M. Goryl, P. Piatkowski, M. Szymonski, Phys. Rev. B **77**, 235427 (2008). https://doi.org/10.1103/PhysRevB.77.235427
57. K. Sajewicz, F. Krok, J. Konior, Jpn. J. Appl. Phys. **49**(2), 025201 (2010). https://doi.org/10.1143/JJAP.49.025201
58. Y. Rosenwaks, R. Shikler, T. Glatzel, S. Sadewasser, Phys. Rev. B **70**, 085320 (2004)
59. G. Enevoldsen, T. Glatzel, M. Christensen, J. Lauritsen, F. Besenbacher, Phys. Rev. Lett. **100**, 236104 (2008). https://doi.org/10.1103/PhysRevLett.100.236104
60. R. Jöhr, A. Hinaut, R. Pawlak, A. Sadeghi, S. Saha, S. Goedecker, B. Such, M. Szymoski, E. Meyer, T. Glatzel, J. Chem. Phys. **143**(9), 094202 (2015). https://doi.org/10.1063/1.4929608
61. S. Kawai, T. Glatzel, H.J. Hug, E. Meyer, Nanotechnology **21**(24), 245704 (2010)
62. F. Bocquet, L. Nony, C. Loppacher, T. Glatzel, Phys. Rev. B **78**, 035410 (2008). https://doi.org/10.1103/PhysRevB.78.035410
63. T. Hochwitz, A. Henning, C. Levey, C. Daghlian, J. Slinkman, J. Vac. Sci. Technol. B **14**(1), 457 (1996)
64. G. Elias, T. Glatzel, E. Meyer, A. Schwarzman, A. Boag, Y. Rosenwaks, Beilstein J. Nanotechnol. **2**, 252 (2011). https://doi.org/10.3762/bjnano.2.29
65. R. Dianoux, F. Martins, F. Marchi, C. Alandi, F. Comin, J. Chevrier, Phys. Rev. B **68**, 045403 (2003). https://doi.org/10.1103/PhysRevB.68.045403